ChemComm

COMMUNICATION

View Article Online
View Journal

Cite this: DOI: 10.1039/d6cc01648k

Received 18th March 2026,
Accepted 20th May 2026

DOI: 10.1039/d6cc01648k

rsc.li/chemcomm

Evolving a fluorescent light-up aptamer for rotationally quenched asymmetric rhodamines

Franziska Grün,† Daniel Englert,† Andrijana Crenner, Sven Jänner, Eva-Maria Burger, Murat Sunbul * and Andres Jäschke *

We describe the evolution and characterization of a fluorescent light-up aptamer, RhoBAST^{G36C}, that binds asymmetric, rotationally quenched rhodamines. Binding induces an over 300-fold fluorescence turn-on, which we leveraged for real-time monitoring *in vitro* transcription reactions and live-cell imaging of tRNA and mRNA in *E. coli*.

Fluorescence microscopy is a key technique for studying biomolecules within their cellular context, providing valuable insight into their functions. Although RNA plays a central role in virtually all aspects of cell biology, tools for live-cell visualization of RNA have lagged behind those developed for protein imaging. This gap largely arises from the absence of genetically encoded and inherently fluorescent RNAs. The development of protein-based RNA imaging systems such as MS2[1] and PP7[2] as well as more recently developed fluorescent light-up aptamers (FLAPs) have significantly advanced the RNA imaging toolbox. FLAPs combine the fluorogenicity of small-molecule fluoro-phores with the genetic encodability of the aptamer fused to the RNA of interest.

The mechanisms underlying dye fluorogenicity are diverse and include fluorophore dimerization,[3,4] attachment of quencher moieties,[5,6] environment-dependent spirocyclization,[7,8] and intramolecular motion.[9,10] Notably, a particular focus within the latter category is rotational relaxation within the dye molecule, often through single bonds.[11,12] Despite its potential, this mechanism has been relatively underexplored. A recent study introduced a julolidine-based fluorescent molecular rotor in conjunction with its binding partner, the Okra aptamer, enhancing FLAP-based RNA imaging in the green spectral range, and offering a brighter and more photostable alternative to existing Broccoli and Pepper systems.[13] Another study using orange-red fluorescent *N*-aryl-substituted sulforhodamines demonstrated only modest aptamer affinity, limiting advancements in high-resolution imaging applications.[14] Beyond FLAPs, asymmetric rhodamines have been utilized as viscosity-sensitive probes and for targeting cell organelles such as mitochondria and lysosomes based on pH values.[15,16]

The rhodamine-binding aptamer for super-resolution imaging techniques (RhoBAST) is an exceptionally performant FLAP, distinguished by its photostability, high affinity, and brightness, making it ideal for super-resolved RNA imaging in live cells.[17] Its compatibility with a broad range of xanthene-based dyes, due to its promiscuity, further enhances its utility across various fluorogens.[7,18] So far, RhoBAST's fluorogenicity has been induced by attached quenchers (Fig. 1A i),[17] dimerization,[3] and spirocyclization (Fig. 1A ii).[7] Furthermore, its robustness allows it to be combined with protein binding aptamers, expanding the scope of targetable biomolecules.[7,19]

In this work, we explore a light-up strategy based on restricting intramolecular motion, particularly the rotation, of rhodamine fluorophores (Fig. 1A iii). We first tested whether a modified rhodamine dye could be bound by RhoBAST. To this end, a phenyl ring was introduced to one of the exocyclic amines of TMR, yielding the asymmetric phenyltrimethyl rhodamine, **PhTMR** (Fig. 1A iii). This structural modification facilitates rotational relaxation, rendering the dye quenched in solution.[11] *In vitro*, binding to RhoBAST efficiently suppressed the rotation around the N–C_{aryl} bond, resulting in a fluorescence turn-on of (257 ± 5)-fold. This performance compares favorably with contact-quenched TMR-DN (27-fold) and spirocyclization-based SpyRho (60-fold) (Fig. S1A). However, the binding affinity of RhoBAST with PhTMR, with a dissociation constant (K_D) of 360 ± 13 nM, was more than 10-fold weaker than for TMR-DN (15 nM) and SpyRho (34 nM) (Fig. S1B, Table S1), indicating the need for aptamer improvement through reselection. To achieve this, we performed an *in vitro* SELEX experiment, immobilizing **PhTMR** *via* triethylene glycol diamine (H_2N–$(PEG)_2$–NH_2) linker on NHS-activated Sepharose beads, yielding **3** (Fig. 1B and Scheme S1). The initial RNA library was a doped version based on RhoBAST, with each nucleotide position mutated at 15%, resulting in a diversity of about 4×10^{14} sequences. The doped RhoBAST sequence was flanked by constant primer regions for amplification (Fig. 1C). Prior to each selection round, an incubation with a mock resin, conjugated with only linker (H_2N–$(PEG)_2$–NH_2),

Institute of Pharmacy and Molecular Biotechnology (IPMB), Heidelberg University, Heidelberg, Germany. E-mail: msunbul@uni-heidelberg.de, jaeschke@uni-hd.de
† Authors declare shared first-authorship.

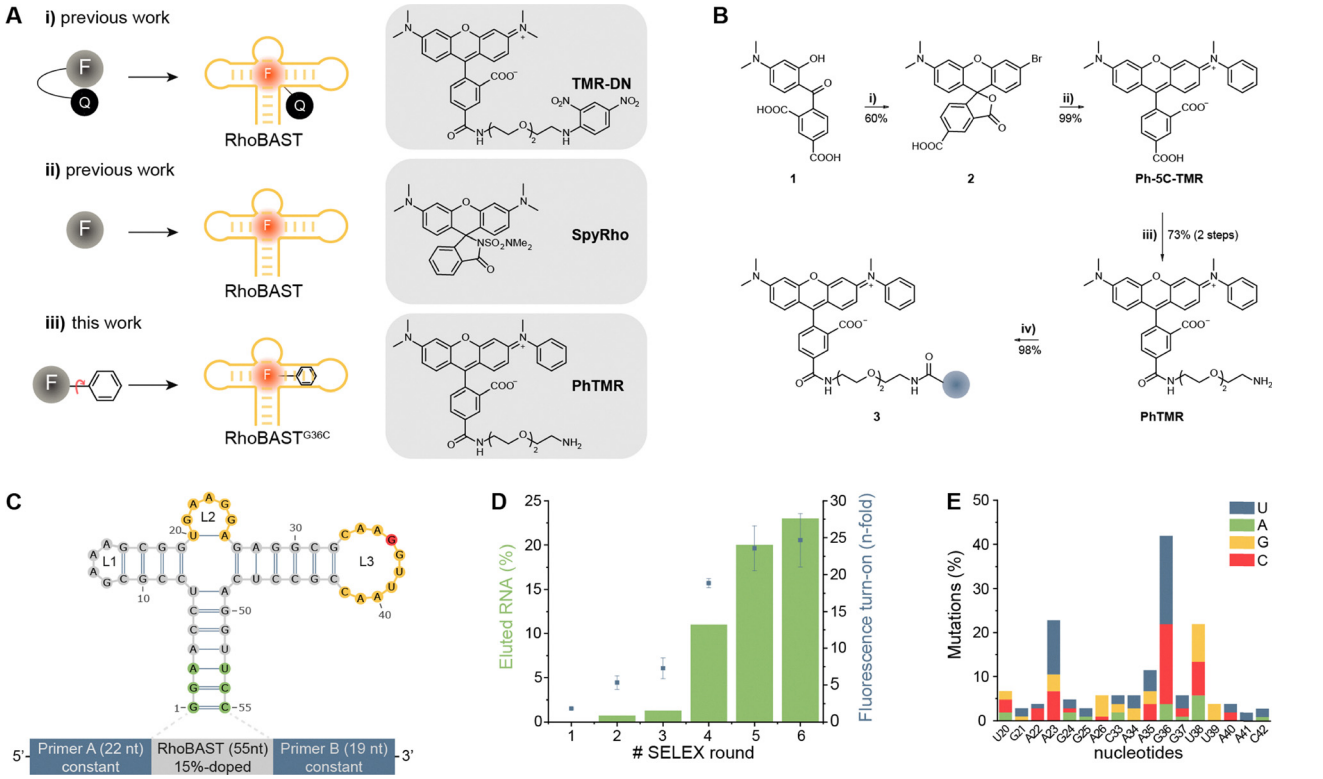

Fig. 1 Evolution of PhTMR-binding aptamer RhoBAST^{G36C}. (A) Schematic drawing and chemical structure of (i) previous work using contact-quenched tetramethyl rhodamine with attached dinitroaniline, TMR-DN, lighting up upon binding to RhoBAST, (ii) previous work using environment-dependent spirocyclic rhodamine, SpyRho, lighting up upon binding to RhoBAST and (iii) this work using PhTMR which is quenched by rotational relaxation and lights up by interaction with the evolved aptamer, RhoBAST^{G36C}. (B) Synthesis of PhTMR and immobilization on solid phase. (i) 3-Bromophenol, TFA, $MeSO_3H$, (ii) *N*-methylaniline, $ZnCl_2$, (iii) amide-coupling to H_2N-$(PEG)_2$NHBoc using PyBOP, DIPEA, DMF; deprotection using HCl, dioxane, (iv) NHS-activated Sepharose resin, HEPES buffer (100 mM, pH 7.4). (C) Design of the RNA SELEX library based on the sequence of RhoBAST (15% doped) flanked by constant primer regions. Nucleotides (nt) highlighted in green were non-doped nucleotides. Loop 2 (L2) and Loop 3 (L3) were highly conserved regions in previous selections.[17,20] (D) Enrichment of the RNA pool through SELEX observed as percentage of eluted RNA and as fluorescence increase (turn-on) by incubation of RNA pool (100 nM) with PhTMR (36 nM). (E) Observed mutation rates after six rounds of SELEX in the previously conserved loop regions (L2: nt #20–26, L3: nt #33–42).

was performed to remove nonspecific binders. The SELEX process involved incubation with the immobilized target, removal of non-binders, elution of binders, RT-PCR amplification, and *in vitro* transcription. After six rounds, enrichment was evident from the increased amount of eluted RNA and fluorescence activation (Fig. 1D). Sanger sequencing resulted in 105 mutants, which were aligned, and the occurrence of mutations at each position was analyzed (Tables S6 and S7). This revealed high mutation frequencies at positions 23, 36, and 38 within the loops L2 and L3, consistent with previous studies (Fig. 1C and E).[17,20] With the prediction of secondary structures[21] of all mutants, 41 sequences were identified exhibiting a RhoBAST-like folding (Table S8). Here, quantification of mutations and *in vitro* mutagenesis highlighted position 36 as a key site (Tables S1 and S8). Substituting guanine with pyrimidines at this position significantly improved affinity: the G36U mutant showed a K_D of 247 ± 23 nM and the G36C mutant exhibited a K_D of 115 ± 7 nM, more than three times better than parental RhoBAST (360 ± 13 nM) or the G36A mutant (384 ± 22 nM) (Fig. S1B and Table S1). Notably, the G36C mutant achieved an exceptional fluorescence turn-on of 309-fold, surpassing previous RhoBAST systems based on SpyRho and TMR-DN by 5- and 11-fold, respectively (Fig. S1A). Thus, the reselection yielded RhoBAST^{G36C} as novel rotationally quenched rhodamine-binding aptamer (Fig. S1D). The importance of position 36 aligns with recent crystal structures of RhoBAST bound to TMR-DN and SpyRho, which reveal an A-like architecture with a semi-open binding pocket.[22,23] Specifically, G18-A35-A28 form the pocket's floor, while the xanthene core stacks on A22-A40.[23] The low mutation rates at these positions indicate structural conservation. In contrast, the G36-U39 turn region, which encapsulates the dye,[23] was highly mutable, allowing adaptation without disrupting the overall folding structure (Fig. 1E). RhoBAST^{G36C}:PhTMR shows high fluorescence intensity within physiologically relevant magnesium concentrations[24] (Fig. S1E) and exhibits excitation (574 nm) and emission maxima (606 nm) compatible with standard fluorescence microscopy setups (Fig. S1F). Following the successful selection of RhoBAST^{G36C} against the phenyl-substituted rhodamine, we aimed to expand the dye scope by synthesizing probes with diverse aryl moieties. These variations were designed to probe how electronic and steric effects influence performance. To streamline derivatization, the different aryl substituents were introduced in the final synthetic step (Scheme S1B). Specifically, the asymmetrical bromo-substituted rhodamine core was synthesized and subsequently converted into the aryl-substituted probes (Fig. 2A) *via* zinc-mediated

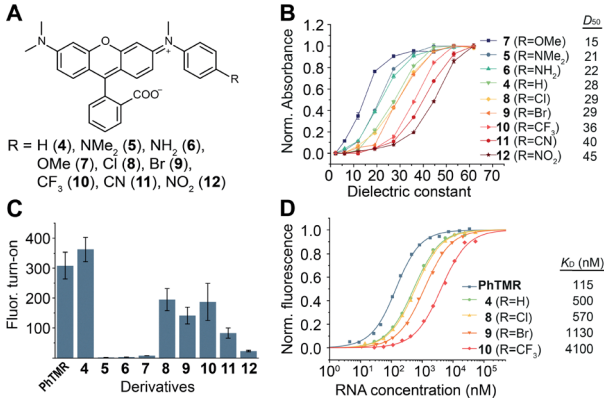

Fig. 2 Characterization of aryl rhodamine derivatives. (A) Chemical structure of synthesized aryl rhodamines with different residues (R). (B) Normalized absorbance of aryl-substituted rhodamines (5 μM) depending on the dielectric constant of the respective solvent mixture (water/dioxane) yielding D_{50} values. (C) Fluorescence turn-on of aryl rhodamines (1 μM) with RhoBAST^{G36C} (5 μM). Values are given as mean ± s.d. (N = 3 independent measurements). (D) Dissociation constants (K_D) were obtained by measuring fluorescence increase upon titration of aryl rhodamine derivatives (50 nM) with increasing concentrations of RhoBAST^{G36C}.

nucleophilic aromatic substitution or Buchwald–Hartwig coupling (Scheme S1B). This yielded nine derivatives (Fig. 2A, SI Chemical Synthesis). All derivatives exhibited comparable absorption and emission maxima (Table S2). As previously observed,[7,25] binding of the rhodamine derivatives to the aptamer led to a bathochromic shift towards higher wavelengths in both the excitation ($\Delta_{batho.ex}$ 6–36 nm) and emission ($\Delta_{batho.em}$ 6–30 nm) maxima (Table S2). Notably, the Stokes-shifts (derivatives **4–12**: RhoBAST^{G36C} Δ_{Stokes} = 15–36 nm, PhTMR:RhoBAST^{G36C} Δ_{Stokes} = 32 nm) allows good separation of excitation and emission light with standard fluorescence microscopy setups (Table S2). While spirocyclization of previous light-up rhodamines was influenced by electron-deficient substituents at the 3-position (Fig. 1A ii),[7] here we investigated the impact of various aryl residues on the spirolactonization (Fig. S2A). The D_{50} values, given as the dielectric constant of the water–dioxane solvent mixture at the half-maximum absorbance, were strongly dependent on the electronic nature of the substituents (Fig. 2B and Table S2). Electron-donating groups (derivatives **5–7**) shifted the equilibrium towards the quinoid form, resulting in lower D_{50} values (D_{50} = 15–22), while electron withdrawing groups (derivatives **8–12**) favored the spirolactone form, yielding higher D_{50} values (D_{50} = 29–45), relative to unsubstituted phenyl rhodamine **4** (D_{50} = 28) (Table S2). These D_{50} values correlated with the Hammett parameter (σ) of the substituents (Fig. S2B). We then evaluated fluorescence turn-on upon interaction with RhoBAST^{G36C} (Fig. 2C). Derivatives **5–7**, **11** and **12** showed minimal turn-ons and were excluded from further analysis (Fig. The remaining derivatives, exhibiting more than 140-fold fluorescence enhancement, surpassed the performance of the predecessor systems RhoBAST:TMR-DN (26-fold) and RhoBAST:SpyRho (60-fold) (Fig. S1A and Table S2). The most promising derivatives were further characterized *in vitro*. The dissociation constants (K_D) were determined by titration of a fixed concentration of fluorophore (50 nM) with different aptamer concentrations, measuring the fluorescence increase. The obtained K_D values revealed that increasing the size of the substituent (R = H < Cl < Br < CF_3) as well as increasing D_{50} values (D_{50} H < Cl = Br < CF_3) led to decreasing affinity towards RhoBAST^{G36C} (K_D = 500, 570, 1130, 4100 nM, respectively, Fig. 2D and Table S2). The attachment of the triethylene glycol linker with amine and amide functionality to **4** further increased the affinity (K_D = 115 ± 7 nM for **PhTMR**). This trend aligns with prior reports[26] and highlights how linker conjugation can enhance binding.[17] Quantum yield measurements showed that aryl-substituted rhodamines had very low intrinsic fluorescence in solution due to efficient quenching by rotational relaxation. Interaction with RhoBAST^{G36C} increased the quantum yield by over 100-fold, resulting in high brightness (Table S3). The linear dependence of the quantum yield on the viscosity in water-glycerol mixtures supported the hypothesis that rotation along the N–C_{aryl} bond governs relaxation (Fig. S2C). Finally, the nonspecific light-up of **PhTMR**, **4**, **8–10** with total RNA isolated from *E. coli* and protein (BSA) were compared to the specific light-up with RhoBAST^{G36C} (Fig. S2D). Since **PhTMR** demonstrated minimal nonspecific light-up (Fig. S2D), high brightness (Table S3), strong binding affinity (K_D = 115 nM) and an outstanding fluorescent turn-on (309-fold), it was selected for all subsequent *in vitro* and cellular applications.

Leveraging the high fluorescence turn-on of the RhoBAST^{G36C}:PhTMR system, we established an *in vitro* assay to monitor RNA synthesis in real-time. Using DNA templates encoding RhoBAST^{G36C} or RhoBAST, each carrying a T7-promoter, *in vitro* transcription with T7 polymerase was performed in the presence of the respective fluorogen. The appearance of fluorescence indicated aptamer synthesis (Fig. 3A). As negative control, the orthogonal silicon rhodamine-binding aptamer, SiRA,[26] was transcribed in presence of fluorogen (Fig. 3A). RhoBAST^{G36C}: PhTMR outperformed RhoBAST:TMR-DN, showing a magnitude higher turn-on (Fig. 3A).

We also demonstrated live-cell RNA imaging using the RhoBAST^{G36C} system. Here, a single repeat of the aptamer was fused into the anticodon loop of a tRNA (Fig. S3A). Therewith, confocal imaging of *E. coli* tRNA was achieved in living bacteria (Fig. 3B and Fig. S3C). Next, synonymous aptamer repeats were incorporated into the 3′ untranslated region of plasmids expressing GFP allowing the visualization of GFP mRNA in living *E. coli* (Fig. S3B). Confocal imaging showed bright, specific labeling of GFP mRNA (Fig. 3C and Fig. S3D). As a negative control, the same plasmid without the aptamer was used, resulting in a minimal fluorescent signal of PhTMR.

We determined exceptionally fast exchange kinetics of RhoBAST^{G36C}:PhTMR yielding an association rate coefficient (k_a) of 1.31 × 10^8 M^{-1} s^{-1} and a dissociation rate coefficient (k_d) of 29.7 s^{-1}, as determined by stopped-flow spectrometry (Fig. S4 and Table S4). These rapid kinetics, magnitudes faster than existing FLAP systems,[10,27] make it a promising candidate for single-molecule localization microscopy (SMLM). At a dye concentration of 100 nM, it exhibited a blinking interval 4–9-fold shorter (Table S4) than its predecessor RhoBAST with TMR-DN[17] or SpyRho,[7] potentially facilitating faster acquisition of super-resolved images by SMLM.

Harnessing rotational quenching of aryl-substituted rhodamines, we developed a FLAP system with exceptional fluorescence turn-on. We elucidated how structural and electronic

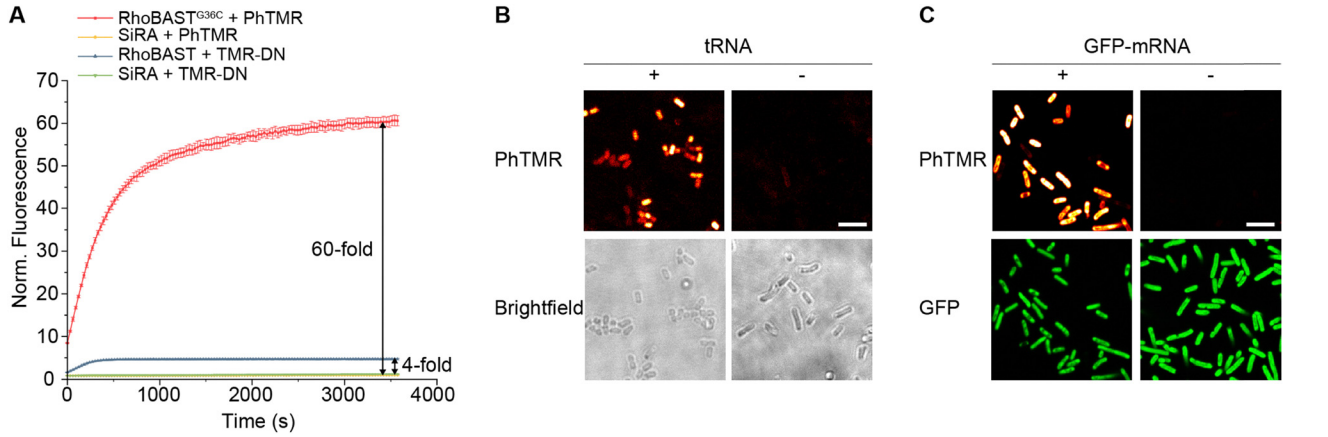

Fig. 3 Application of RhoBAST^{G36C}:PhTMR. (A) Monitored *in vitro* transcription of RhoBAST^{G36C} and RhoBAST using PhTMR (500 nM) and TMR-DN (500 nM), respectively. As negative control, SiRA was transcribed in the presence of PhTMR (500 nM) or TMR-DN (500 nM). Data points represent mean ± s.d. (N = 3 independent experiments) and were normalized. (B) Confocal images of live *E. coli.* tRNA was visualized using 1xRhoBAST^{G36C} (+) with PhTMR (1 μM). As negative control 0xRhoBAST^{G36C} (–) with PhTMR was used. Scale bar, 5 μm. (C) Confocal images of live *E. coli.* GFP mRNA was visualized using 16xRhoBAST^{G36C} (+) with PhTMR (2 μM). As negative control 0xRhoBAST^{G36C} (–) with PhTMR was used. Scale bar, 5 μm.

variations of such rhodamines influence their properties. The demonstrated capabilities of RhoBAST^{G36C}:PhTMR for imaging in living bacteria and the rapid exchange kinetics highlight its potential for advanced applications.

F. G., D. E., M. S., and A. J. designed the study. F. G., D. E., A. C., S. J., and E.-M. B. performed the experiments and data analysis. F. G. wrote the original draft, and all authors contributed to review and editing of the manuscript.

Conflicts of interest

There are no conflicts to declare.

Data availability

The data supporting this article have been included as part of the supplementary information (SI). Supplementary information: detailed materials and methods, supporting figures and tables including spectroscopic and microscopy results, chemical synthesis including analytical data. See DOI: https://doi.org/10.1039/d6cc01648k.

Acknowledgements

This work was supported by the Deutsche Forschungsgemeinschaft (DFG grant no. Ja794/11) and by the Baden-Württemberg Stiftung (MET-ID21-Aptamer-PAINT). The authors thank the Nikon Imaging Center, Heidelberg University, for access and microscopy support. We thank M. Mayer and L. Rohland (ZMBH, Heidelberg University) for assistance with stopped-flow experiments.

References

1 E. Bertrand, P. Chartrand, M. Schaefer, S. M. Shenoy, R. H. Singer and R. M. Long, *Mol. Cell*, 1998, **2**, 437–445.
2 B. Wu, J. Chen and R. H. Singer, *Sci. Rep.*, 2014, **4**, 3615.
3 B. Bühler, J. Schokolowski, A. Benderoth, D. Englert, F. Grün, A. Jäschke and M. Sunbul, *Nat. Chem. Biol.*, 2023, **19**, 478–487.
4 F. Bouhedda, K. T. Fam, M. Collot, A. Autour, S. Marzi, A. Klymchenko and M. Ryckelynck, *Nat. Chem. Biol.*, 2020, **16**, 69–76.
5 M. Sunbul and A. Jäschke, *Angew. Chem.*, 2013, **125**, 13643–13646.
6 E. Braselmann, A. J. Wierzba, J. T. Polaski, M. Chromiński, Z. E. Holmes, S.-T. Hung, D. Batan, J. R. Wheeler, R. Parker and R. Jimenez, *Nat. Chem. Biol.*, 2018, **14**, 964–971.
7 D. Englert, E.-M. Burger, F. Grün, M. S. Verma, J. Lackner, M. Lampe, B. Bühler, J. Schokolowski, G. U. Nienhaus and A. Jäschke, *Nat. Commun.*, 2023, **14**, 3879.
8 S. Fürbacher, P. Doll, J. Zhang, L. Lange, N. van den Bergh, Y. Zhang, E. Vitiello, F. Grün, M. Sunbul and A. Jäschke, *J. Am. Chem. Soc.*, 2026, **148**, 2405–2418.
9 J. S. Paige, K. Y. Wu and S. R. Jaffrey, *Science*, 2011, **333**, 642–646.
10 X. Chen, D. Zhang, N. Su, B. Bao, X. Xie, F. Zuo, L. Yang, H. Wang, L. Jiang and Q. Lin, *Nat. Biotechnol.*, 2019, **37**, 1287–1293.
11 E. M. Kosower, *Acc. Chem. Res.*, 1982, **15**, 259–266.
12 A. Granzhan, H. Ihmels and G. Viola, *J. Am. Chem. Soc.*, 2007, **129**, 1254–1267.
13 F. Zuo, L. Jiang, N. Su, Y. Zhang, B. Bao, L. Wang, Y. Shi, H. Yang, X. Huang and R. Li, *Nat. Chem. Biol.*, 2024, **20**, 1272–1281.
14 J. Lee, K. H. Lee, J. Jeon, A. Dragulescu-Andrasi, F. Xiao and J. Rao, *ACS Chem. Biol.*, 2010, **5**, 1065–1074.
15 P. Tang, Q. Wang, Q. Tan, K. Huang, B. Du and L. Liang, *Microchem. J.*, 2023, **194**, 109296.
16 Y. Zhou, Q. Wang, S. Chanmungkalakul, X. Wu, H. Xiao, R. Miao, X. Liu and Y. Fang, *Chem. – Eur. J.*, 2024, **30**, e202303707.
17 M. Sunbul, J. Lackner, A. Martin, D. Englert, B. Hacene, F. Grün, K. Nienhaus, G. U. Nienhaus and A. Jäschke, *Nat. Biotechnol.*, 2021, **39**, 686–690.
18 M. Sunbul and A. Jäschke, *Nucleic Acids Res.*, 2018, **46**, e110–e110.
19 F. Grün, N. van den Bergh, M. Klevanski, M. S. Verma, B. Bühler, G. U. Nienhaus, T. Kuner, A. Jäschke and M. Sunbul, *Angew. Chem.*, 2024, e202412810.
20 L. A. Holeman, S. L. Robinson, J. W. Szostak and C. Wilson, *Folding Des.*, 1998, **3**, 423–431.
21 M. Zuker, *Nucleic Acids Res.*, 2003, **31**, 3406–3415.
22 Y. Zhang, Z. Xu, Y. Xiao, H. Jiang, X. Zuo, X. Li and X. Fang, *Nat. Commun.*, 2024, **15**, 4206.
23 S. H. Siwik, A. J. Wierzba, S. R. Lennon, L. T. Olenginski, A. E. Palmer and R. T. Batey, *Nucleic Acids Res.*, 2025, **53**, gkaf555.
24 R. D. Grubbs, *BioMetals*, 2002, **15**, 251–259.
25 L. Gu, J. Zheng, Y. Zhang, D. Wang and J. Liu, *Chem. – Eur. J.*, 2023, **29**, e202302616.
26 R. Wirth, P. Gao, G. U. Nienhaus, M. Sunbul and A. Jäschke, *J. Am. Chem. Soc.*, 2019, **141**, 7562–7571.
27 X. Li, H. Kim, J. L. Litke, J. Wu and S. R. Jaffrey, *Angew. Chem., Int. Ed.*, 2020, **59**, 4511–4518.